Journal of Sound and Vibration (1999) **221**(5), 823–848
Article No. jsvi.1998.2035, available online at http://www.idealibrary.com on IDEAL

DYNAMICS OF A SLENDER BEAM WITH AN ATTACHED MASS UNDER COMBINATION PARAMETRIC AND INTERNAL RESONANCES PART I: STEADY STATE RESPONSE

S. K. Dwivedy and R. C. Kar
Department of Mechanical Engineering, Indian Institute of Technology, Kharagpur 721 302, *India*

(*Received* 15 *September* 1997, *and in final form* 28 *September* 1998)

The non-linear behaviour of a slender beam with an attached mass at an arbitrary position under vertical base excitation is investigated with combination parametric and internal resonances. The governing equation which retains the cubic non-linearities of geometric and inertial type is discretized by using Galerkin's method and the resulting second order temporal differential equation is then reduced by the method of multiple scales to a set of first order non-linear differential equations. Steady state response and its stability are obtained numerically from these reduced equations. Super- and sub-critical Hopf bifurcations in the trivial as well as non-trivial branches and the saddle-node or fold type bifurcations in the non-trivial branches of the response curves are found. The effect of damping, amplitude as well as frequency of base excitation, the mass ratio and the location of the concentrated mass on the non-linear response of the system having internal resonance of 3:1 is studied at length. Hysteresis, saturation and blue sky catastrophe phenomena with bistability interval in the response curves are observed for a wide range of bifurcating parameters.

1. INTRODUCTION

Many mechanical members can be modelled as a cantilever beam with an attached mass subjected to base excitation at a frequency in the neighbourhood of the sum of the frequencies of the lower two modes. Such a system is said to be under combination parametric resonance and has been studied by many researcher [1–5]. Most of these cases are characterized by linear Mathieu–Hill equations and a few of them are of Duffing type Mathieu–Hill equations [6–9]. Asmis and Tso [10] analyzed the response of two-degree-of freedom systems with cubic non-linearities to a combination parametric resonance in the presence of one-to-one internal resonances. They found that internal resonance reinforces the combination resonant response and investigated the influence of detuning on the response. Tezak *et al*. [11] studied a clamped–clamped beam with cubic

0022–460X/99/150823 + 26 $30.00/0

geometrical non-linearities under combination parametric excitation in the presence of internal resonance of type three-to-one. Nayfeh [12] and Nayfeh and Jebrill [13] investigated the response of two-degree-of-freedom systems with quadratic non-linearities to parametric excitation. Nayfeh [14] considered the response of multi-degree-of-freedom systems with quadratic non-linearities to a harmonic parametric excitation in the presence of an internal resonance of the combination type. Cartmell and Roberts [15] studied simultaneous combination resonances in an autoparametrically resonant system.

Nayfeh and Zavodney [16] dealt with the response of two-degree-of-freedom systems with quadratic non-linearities to a combination parametric resonance and found that, in addition to the trivial and non-trivial steady state responses, periodic solution and Hopf bifurcation exist in the non-trivial branches. Streit *et al.* [17] analyzed combination parametric resonance leading to periodic and chaotic response in two-degree-of freedom systems with quadratic non-linearities in the presence of one-to-two internal resonances. Systems having quadratic or cubic non-linearities with internal resonances experiencing external excitation exhibit multi-valued steady state response, turning point bifurcation, periodic response and period-doubling bifurcation leading to chaos [5].

To date simultaneous parametric and internal resonance cases are limited to the systems like hinged–clamped beam [11] (3:1 internal resonance and cubic geometric non-linearities), coupled bending–torsion vibration of cantilever beam [18] and auto-parametric vibration of two- or three-beam structures with concentrated masses [15]. For a simple base excited cantilever beam with a concentrated mass, Kar and Dwivedy [19] found that, for certain values of mass ratios (i.e., the ratio of the concentrated mass to the mass of the beam) and/or location of the attached mass, internal resonance of three-to-one is possible and investigated many interesting chaotic phenomena in addition to periodic, quasiperiodic and fixed point responses for principal parametric resonance only. The present work is concerned with the non-linear steady state response of the previous system to combination parametric and internal resonances. The method of multiple scales and suitable numerical techniques are used to study the resonant behaviour of the system.

2. ANALYSIS

2.1. EQUATION OF MOTION

The equation of motion of a uniform cantilever beam of length L carrying a mass m at an arbitrary position d from the fixed end and subjected to base motion (Figure 1) can be given by [20]

$$EI\left\{v_{ssss}+\frac{1}{2}v_s^2 v_{ssss}+3v_s v_{ss}v_{sss}+v_{ss}^3\right\}+\left(1-\frac{1}{2}v_s^2\right)\{[\rho+m\delta(s-d)]v_{tt}+cv_t\}$$
$$+v_s v_{ss}\int_s^L\{[\rho+m\delta(\xi-d)]v_{tt}+cv_t\}\mathrm{d}\xi-[J_0\delta(s-d)(v_s)_{tt}]_s-(Nv_s)_s=0, \quad (1)$$

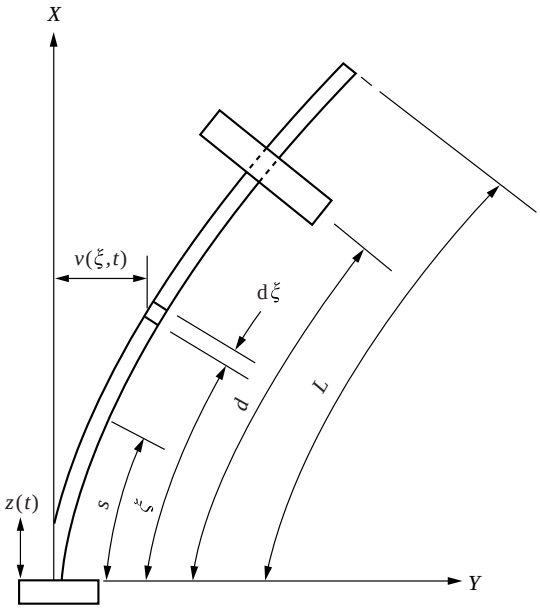

Figure 1. Vertically base-excited cantilever beam carrying a lumped mass.

subject to the boundary conditions

$$v(0,t)=0, \quad v_s(0,t)=0, \quad v_{ss}(L,t)=0, \quad v_{sss}(L,t)=0, \tag{2}$$

where

$$\begin{aligned} N=&\frac{1}{2}\rho\int_s^L\left\{\int_s^\xi (v_s^2)_{tt}\,\mathrm{d}\eta\right\}\mathrm{d}\xi+\frac{1}{2}m\int_s^L\delta(\xi-d)\left\{\int_0^\xi (v_s^2)_{tt}\,\mathrm{d}\eta\right\}\mathrm{d}\xi\\ &+m(z_{tt}-g)\int_s^L\delta(\xi-d)\,\mathrm{d}\xi+\rho L\left(1-\frac{s}{L}\right)(z_{tt}-g)\\ &-J_o\,\delta(s-d)\{1/2v_{stt}v_s^2+v_sv_{st}^2\}, \end{aligned} \tag{3}$$

with the notation

$$(\,)_t=\frac{\partial(\,)}{\partial t}, \quad (\,)_s=\frac{\partial(\,)}{\partial s} \quad \text{etc.}$$

E, I and ρ are respectively the Young's modulus, the second moment of area of the cross-section of the beam and mass per unit length of the beam, J_o is the moment of inertia of the concentrated mass m about its centroidal axis perpendicular to the X–Y plane, v is the lateral displacement of the beam, g, c and z are respectively the acceleration due to gravity, the coefficient of viscous damping and the displacement of the base, s is the distance of a point on the beam, measured along the center line of the deflected beam from the base, t is the time and δ is the Dirac delta function.

The assumptions made in the derivation of equation (1) are that the beam is slender and oscillates only in a transverse plane, i.e., no out of plane motion

takes place and the mass is not positioned at the tip as it would violate the fourth boundary condition.

Let the base motion be harmonic, that is

$$z(t) = Z_o \cos \Omega t. \tag{4}$$

Assuming the solution of equation (1) in the form

$$v(s,t) = \sum_{n=1}^{\infty} r\psi_n(s)u_n(t), \tag{5}$$

where r is a scaling factor, $\psi_n(s)$ is the shape function of the *nth* mode (see Appendix), and u_n is the time modulation of the *nth* mode, applying Galerkin's method and using the non-dimensional parameters

$$x = \frac{s}{L}z, \quad \beta = \frac{d}{L}, \quad \tau = \theta_1 t, \quad \omega_n = \frac{\theta_n}{\theta_1},$$
$$\lambda = \frac{r}{L}, \quad \mu = \frac{m}{\rho L}, \ \Gamma = \frac{Z_o}{Z_r}, \quad J = \frac{J_o}{\rho L r^2}, \quad \phi = \frac{\Omega}{\theta_1} \tag{6}$$

we have the temporal form equation (1) as

$$\ddot{u}_n + 2\varepsilon\zeta_n\dot{u}_n + \omega_n^2 u_n - \varepsilon\sum_{m=1}^{\infty} f_{nm}u_m \cos\phi\tau$$
$$+ \varepsilon\sum_{k=1}^{\infty}\sum_{l=1}^{\infty}\sum_{m=1}^{\infty}\{\alpha_{klm}^n u_k u_l u_m + \beta_{klm}^n u_k \dot{u}_l \dot{u}_m + \gamma_{klm}^n u_k u_l \ddot{u}_m\} = 0, \tag{7}$$

where $\dot{(\ )} = \mathrm{d}(\ )/\mathrm{d}\tau$. The coefficients are defined in the Appendix. The small dimensionless parameter ε is introduced as a book-keeping device to indicate the smallness of damping, non-linearities and excitation.

So, one has n number of coupled equations with cubic geometric non-linearity α_{klm}^n and inertial non-linearities $\beta_{klm}^n, \gamma_{klm}^n$, where n represents the number of modes participating in the resulting oscillation, which do not lend to the closed form of solutions. Hence, approximate solutions will be sought by using the method of multiple scales (section 2.3).

2.2. PHYSICAL EXAMPLE

A metallic beam is considered with the following properties: $L = 125$ mm, $I = 0{\cdot}04851$ mm^4, $E = 0{\cdot}20936 \times 10^6$ N/mm^2, $Z_r = 1$ mm, $c = 0{\cdot}1$ N/ s/mm^2, $\rho = 0{\cdot}03332$ gm/mm, $\mu = 3{\cdot}68979$, $J = 0{\cdot}959$, $\beta = 0{\cdot}25$. The roots of the characteristic equation (see Appendix) are found numerically to be $\kappa_1 = 1{\cdot}80097$, $\kappa_2 = 3{\cdot}2836$ and the corresponding non-dimensional natural frequencies are $\omega_1 = 1$ and $\omega_2 = 3{\cdot}33179$. The book-keeping parameter ε and scaling factor λ are taken as $0{\cdot}001$ and $0{\cdot}1$, respectively. The coefficients of damping ζ_n, excitation f_{nm} and non-linear terms, α_{klm}^n, β_{klm}^n, γ_{klm}^n are found to be of the same order. The values of other required parameters expressed in the Appendix are calculated to be: $\alpha_{e11} = 2{\cdot}54149$, $\alpha_{e12} = -12{\cdot}2027$, $\alpha_{e21} = -6{\cdot}63699$, $\alpha_{e22} = -195{\cdot}55$, $Q_{131} =$

14·62282, $Q_{31} = 7{\cdot}84674$, $f^*_{11} = 0{\cdot}2623$, $f^*_{12} = 0{\cdot}048847$, $f^*_{21} = 0{\cdot}16996$, $f^*_{22} = 0{\cdot}6797$, $\zeta^*_1 = 0{\cdot}04756$, $\zeta^*_2 = 0{\cdot}018346$.

2.3. PERTURBATION SOLUTION

The approximate solution of equation (7) can be obtained using the method of multiple scales. Let

$$u_n(\tau;\, \varepsilon) = u_{no}(T_o, T_1) + \varepsilon u_{n1} + \ldots,\ T_o = \varepsilon^0 \tau,\ T_1 = \varepsilon^1 \tau. \tag{8, 9}$$

Substituting equations (8) and (9) into equation (7) and equating the coefficients of ε^0 and ε to zero, we have

$$D_o^2 u_{no} + \omega_n^2 u_{no} = 0 \tag{10}$$

$$\begin{aligned} D_o^2 u_{n1} + \omega_n^2 u_{n1} = -\Bigg[& 2\xi_n D_o u_{no} + 2 D_o D_1 u_{no} \sum_{n,m=1}^{2} f_{nm} u_{mo} \cos\phi\tau \\ & + \sum_{klm} (\alpha^n_{klm} u_{ko} u_{lo} u_{mo} + \beta^n_{klm} u_{ko} D_o u_{lo} D_o u_{mo} + \gamma^n_{klm} u_{ko} u_{lo} D_o^2 u_{mo}) \Bigg] \\ = 0 \end{aligned} \tag{11}$$

where $D_o = \partial/\partial T_o$ and $D_1 = \partial/\partial T_1$. The solution of equation (10) is given by

$$u_{no} = A_n \exp(i\omega_n T_o) + cc, \tag{12}$$

where cc indicates the complex conjugate of the preceding terms. Now to determine u_{n1} one has to consider the particular case of external and internal resonances.

2.4. COMBINATION RESONANCE ($\phi \approx \omega_1 + \omega_2$)

Since $\omega_2 \approx 3\omega_1$, to express the nearness of ϕ to $\omega_1 + \omega_2$ the detuning parameters σ_1 and σ_2 are introduced as

$$\omega_2 = 3\omega_1 + \varepsilon\sigma_2, \quad \phi = 4\omega_1 + \varepsilon\sigma_1 = \omega_1 + \omega_2 + \varepsilon(\sigma_1 - \sigma_2). \tag{13, 14}$$

Substituting equations (12)–(14) into equation (11) and eliminating the secular terms, one has, for $n = 1$,

$$\begin{aligned} & 2i\omega_1(\zeta_1 A_1 + A_1') - \frac{1}{2} f_{12} \bar{A}_2 \exp\{i\varepsilon(\sigma_1 - \sigma_2) T_o\} \\ & \quad + \sum_{j=1}^{2} \alpha_{e1j} A j \bar{A}_j A_1 + Q_{131} A_2 \bar{A}_1^2 \exp(-i\varepsilon\sigma_2 T_o) = 0, \end{aligned} \tag{15}$$

for $n = 2$,

$$2i\omega_2(\zeta_2 A_2 + A_2') - \frac{1}{2} f_{21} \bar{A}_1 \exp\{i\varepsilon(\sigma_1 - \sigma_2)T_o\} + \sum_{j=1}^{2} \alpha_{e2j} Aj\bar{A}_j A_2 + Q_{31} A_1^3 \exp(-i\varepsilon\sigma_2 T_o) = 0, \tag{16}$$

and for $n > 2$,

$$2i\omega_n(\zeta_n A_n + A_n') + \sum_{j=1}^{2} \alpha_{e2j} Aj\bar{A}_j A_2 = 0. \tag{17}$$

As the higher modes ($n > 2$) are neither directly excited nor indirectly excited by internal resonance, they die out due to the presence of damping. So, for this case, our n-dimensional system reduces to a two-dimensional one as modal interaction is limited to two modes only.

Now introducing

$$A_n = \tfrac{1}{2} a_n(T_1) \exp\{i\beta_n(T_1)\}, \tag{18}$$

where a_n and β_n are real, into equations (15) and (16) and separating the results into real and imaginary parts, one has the following set of autonomous equations.

$$2\omega_1(\zeta_1 a_1 + a_1') - \frac{1}{2} f_{12} a_2 \sin\gamma_1 + \frac{1}{4} Q_{131} a_2 a_1^2 \sin\gamma_2 = 0 \tag{19}$$

$$-\omega_1 a_1(\sigma_1 - \gamma_1' - \gamma_2') - f_{12} a_2 \cos\gamma_1 + \frac{1}{2}\sum_{j=1}^{2} \alpha_{e1j} a_j^2 a_1 + \frac{1}{2} Q_{131} a_2 a_1^2 \cos\gamma_2 = 0, \tag{20}$$

$$2\omega_2(\zeta_2 a_2 + a_2') - \frac{1}{2} f_{21} a_1 \sin\ \gamma_1 - \frac{1}{4} Q_{31} a_1^3 \sin\ \gamma_2 = 0 \tag{21}$$

$$-\omega_2 a_2(3\sigma_1 - 4\sigma_2 - \gamma_2' - 3\gamma_1') - f_{21} a_1 \cos\gamma_1 + \frac{1}{2}\sum_{j=1}^{2} \alpha_{e2j} a_j^2 a_2, + \frac{1}{2} Q_{31} a_1^3 \cos\gamma_2 = 0, \tag{22}$$

where

$$\gamma_1 = -\beta_1 + \frac{1}{4}\sigma_1 T_1, \quad \gamma_2 = -\beta_2 - \left(\sigma_2 T_1 - \frac{3}{4}\sigma_1 T_1\right). \tag{23, 24}$$

Since, for steady state $a_1' = a_2' = \gamma_1' = \gamma_2' = 0$, equations (19)–(22) yield

$$2\omega_1\zeta_1 a_1 - \frac{1}{2} f_{12} a_2 \sin\gamma_1 + \frac{1}{4} Q_{131} a_2 a_1^2 \sin\gamma_2 = 0, \tag{25}$$

$$-\omega_1 a_1\sigma_1 - f_{12}a_2\cos\gamma_1 + \frac{1}{2}\sum_{j=1}^{2}\alpha_{e1j}a_j^2 a_1 + \frac{1}{2}\,Q_{131}a_2a_1^2\cos\gamma_2 = 0, \tag{26}$$

$$2\omega_2\zeta_2 a_2 - \frac{1}{2}\,f_{21}\,a_1\sin\gamma_1 - \frac{1}{4}\,Q_{31}a_1^3\sin\gamma_2 = 0, \tag{27}$$

$$-\omega_2 a_2(3\sigma_1 - 4\sigma_2) - f_{21}a_1\cos\gamma_1 + \frac{1}{2}\sum_{j=1}^{2}\alpha_{e2j}a_j^2 a_2 + \frac{1}{2}\,Q_{31}a_1^3\cos\gamma_2 = 0. \tag{28}$$

Four types of solutions are possible, namely, $a_1 = a_2 = 0$, $a_1 \neq 0$ and $a_2 \neq 0$, $a_1 \neq 0$ and $a_2 = 0$, $a_1 = 0$ and $a_2 \neq 0$. For the third case,

$$a_1 = \pm\{2\omega_1\sigma_1/\alpha_{e11}\}^{1/2}. \tag{29}$$

For the fourth case,

$$a_2 = \pm\{8\omega_2(3/4\sigma_1 - \sigma_2)/\alpha_{e22}\}^{1/2}. \tag{30}$$

The first order solution of the system can be given by

$$u_1 = a_1\cos\{\bar{\omega}_1\tau - \gamma_1\}, \quad u_2 = a_2\cos\{\bar{\omega}_2\tau - \gamma_2\}, \tag{31, 32}$$

where

$$\bar{\omega}_1 = \omega_1 + \varepsilon\sigma_1/4, \quad \bar{\omega}_2 = 3\bar{\omega}_1. \tag{33, 34}$$

2.5. STABILITY OF STEADY STATE RESPONSE

As the above reduced equations contain terms like $a_1\gamma_1'$ and $a_2\gamma_2'$, the perturbed equations will not contain the perturbations $\Delta\gamma_1'$ or $\Delta\gamma_2'$ for trivial solutions. So, stability of trivial points cannot be obtained by perturbing the above reduced equations. Hence, to overcome this difficulty, introducing the transformation

$$p_i = a_i\cos\gamma_i, \quad q_i = a_i\sin\gamma_i, \tag{35, 36}$$

and carrying out trigonometric manipulations, one arrives at the following normalized reduced equations:

$$2\omega_1\left(p_1' + \zeta_1 p_1 + \frac{1}{4}\sigma_1 q_1\right) - \frac{1}{2}f_{12}q_2 - \frac{1}{4}\sum_{j=1}^{2}\alpha_{e1j}q_1(p_j^2 + q_j^2)$$
$$+ \frac{1}{4}Q_{131}\{q_2(q_1^2 - p_1^2) + 2p_1p_2q_1\} = 0, \tag{37}$$

$$2\omega_1\left(p_1' + \zeta_1 q_1 - \frac{1}{4}\sigma_1 p_1\right) - \frac{1}{2} f_{12} p_2 + \frac{1}{4}\sum_{j=1}^{2} \alpha_{e1j} p_1 (p_j^2 + q_j^2) + \frac{1}{4} Q_{131}\{p_2(p_1^2 - q_1^2) + 2p_1 q_1 q_2\} = 0, \tag{38}$$

$$2\omega_2\left\{p_2' + \zeta_2 p_2 + \left(\sigma_2 - \frac{3}{4}\sigma_1\right) q_2\right\} - \frac{1}{2} f_{21} q_1 - \frac{1}{4} Q_{31}\{q_1(3p_1^2 - q_1^2)\} - \frac{1}{4}\sum_{j=1}^{2} \alpha_{e2j} q_2 (p_j^2 + q_j^2) = 0, \tag{39}$$

$$2\omega_2\left\{q_2' + \zeta_2 q_2 + \left(\sigma_2 - \frac{3}{4}\sigma_1\right) p_2\right\} - \frac{1}{2} f_{21} p_1 + \frac{1}{4} Q_{31}\{p_1(p_1^2 - 3q_1^2)\} + \frac{1}{4}\sum_{j=1}^{2} \alpha_{e2j} p_2 (p_j^2 + q_j^2) = 0. \tag{40}$$

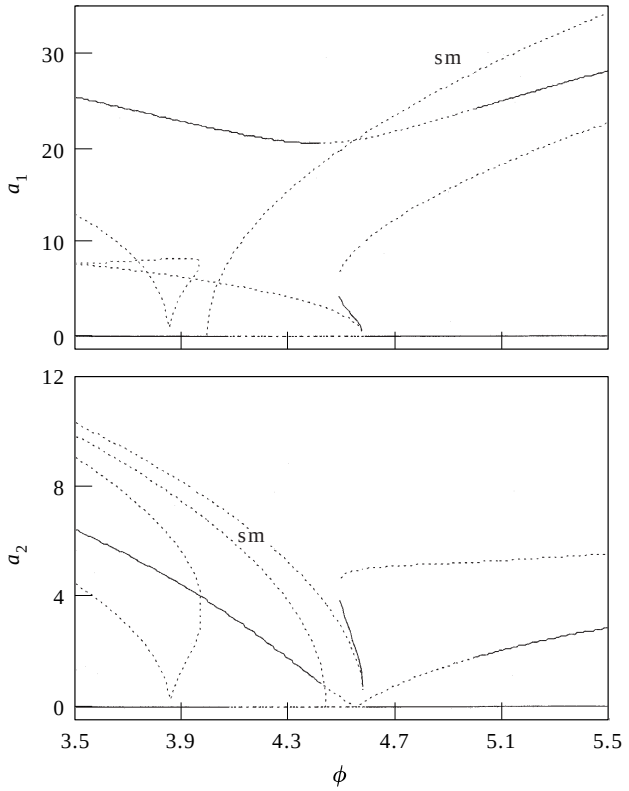

Figure 2. Frequency response curve for undamped system with $\Gamma = 10$, $\mu = 3{\cdot}69$, $\beta = 0{\cdot}25$, $\omega_2 = 3{\cdot}33179$; sm: single mode.

Now perturbing the above equations, one gets

$$\{\Delta p_1',\ \Delta p_2',\ \Delta q_1', \Delta q_2'\}^T = \{J_c\}\{\Delta p_1,\ \Delta p_2,\ \Delta q_1,\ \Delta q_2\}^T, \tag{41}$$

where T is the transpose and J_c is the Jacobian matrix whose eigenvalues will determine the stability of the system. The first order solution of the system in terms of p_n, q_n can be given by

$$u_1 = p_1 \cos \bar{\omega}_1 \tau + q_1 \sin \bar{\omega}_1 \tau, \quad u_2 = p_2 \cos 3\bar{\omega}_1 \tau + q_2 \sin 3\bar{\omega}_1 \tau. \tag{42, 43}$$

3. NUMERICAL RESULTS AND DISCUSSION

Since the system considered contains both cubic geometric (α^n_{klm}) and inertial (β^n_{klm}, γ^n_{klm}) non-linearities, and is subjected to combination parametric resonance along with internal resonance of 3:1, getting a closed-form solution for the steady state response from the reduced equations (25)–(28) having many coupled non-linear terms is very difficult. It may be noted that, with much simpler cases [16, 17], the researchers have gone for a numerical solution to obtain the steady state response curves. Hence, in this case, the non-trivial (n-t) steady state response of the system is obtained by solving the reduced equations (25)–(28)

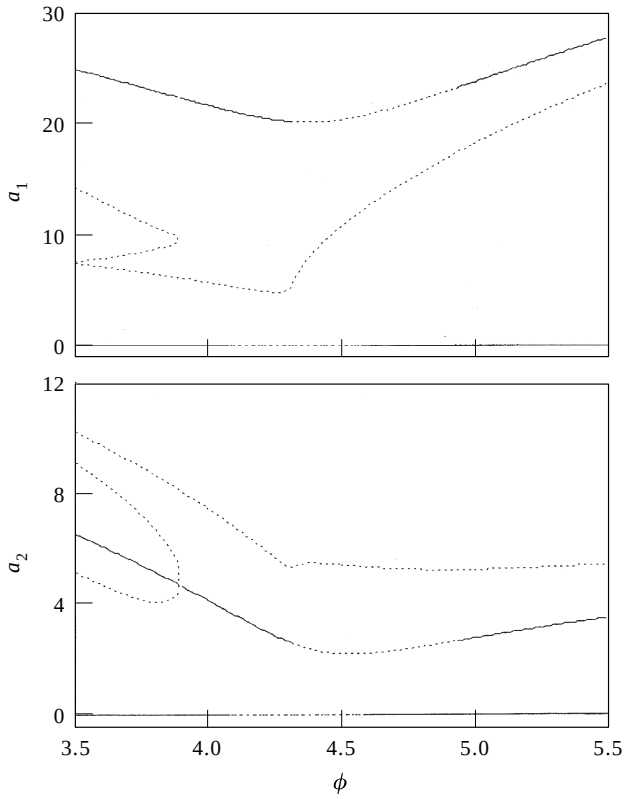

Figure 3. Frequency response curve for $\nu = 2$; key as in Figure 2.

numerically using Newton's method [21] and the stability and bifurcation of the trivial and n-t responses are studied from the eigenvalues of the Jacobian matrix J_c. Here, the effects of damping ν, amplitude Γ and frequency ϕ of base excitation, position β of an attached mass and mass ratio μ on the system response are studied. In the frequency and force response plots the stable and unstable branches are indicated respectively by solid and broken lines.

From equations (33) and (34), it is clear that the first mode will oscillate at a frequency of $\bar{\omega}_1 = \omega_1 + \varepsilon\sigma_1/4$ and the second mode will oscillate at a frequency exactly three times that of the first one. Hence, a *fractional harmonic pair* of (1/4, 3/4) is observed in the system response. Except for Figures 8–11, all other figures are obtained with the data given in section 2.2. In Figures 8–11 the non-linear, forcing and damping terms are obtained from the expressions in the Appendix for the given system parameters μ, β and J.

The steady state frequency response curve for undamped system with $\Gamma = 10$ is shown in Figure 2. The trivial solution becomes unstable between $\phi = 4{\cdot}082$ and $4{\cdot}5814$ with the end points having super- and sub-critical Hopf bifurcation (HB) respectively. A very typical pitchfork type bifurcation occurs at $\phi = 4{\cdot}0$ for the first mode and at $\phi = 4{\cdot}4405$ for the second mode where symmetry breaking takes place without change of stability. These two curves are obtained assuming no energy transfer between the participating modes, i.e., only single mode

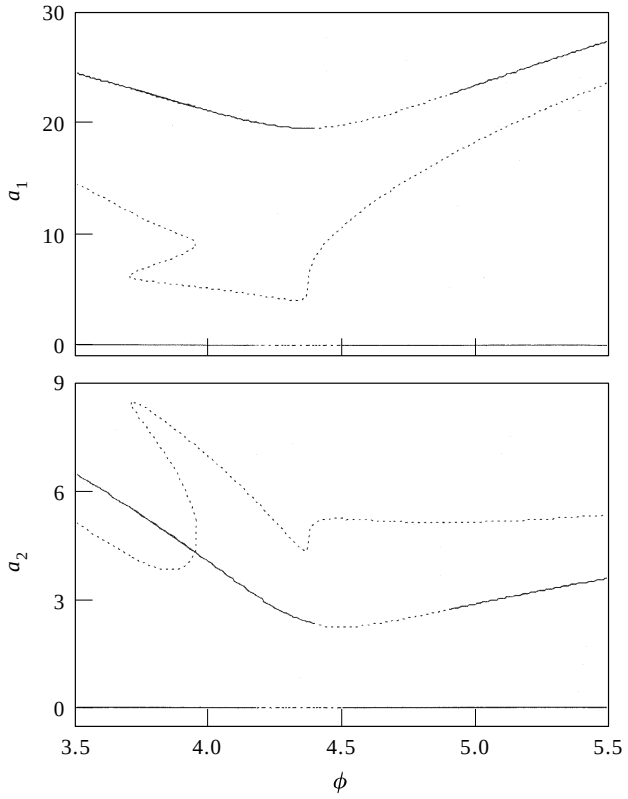

Figure 4. Frequency response curve for $\zeta_1 = \zeta_2 = \zeta_1^* \nu$; key as in Figure 3.

oscillation takes place while the amplitude of the other mode is zero with arbitrary phase combination. This case is not possible with the problems treated by Nayfeh and Zavodney [16], and Streit *et al.* [17], where the solutions are either trivial ($a_1 = a_2 = 0$) or non-trivial ($a_1 \neq 0$, $a_2 \neq 0$). The response curves obtained from equations (29) and (30) are found to be unstable and physically unattainable. Hence, the single mode bifurcating branches are not plotted in the subsequent force or frequency response curves.

For the n-t branches of the response curve, HBs occur at $\phi = 4{\cdot}425$ and $\phi = 4{\cdot}99$ and a saddle-node (s-n) bifurcation occurs at $\phi = 4{\cdot}482$. One may observe the jump-up from the trivial response at $\phi = 4{\cdot}082$ and a jump down from the n-t response at $\phi = 4{\cdot}99$. Though the system is excited at a frequency near about $\omega_1 + \omega_2$, the response amplitude of the first mode dominates that of the second mode. There are many other turning points in the unstable branches which are not s-n bifurcation points as no stability change takes place at those points.

It may be noted that the stability and bifurcation of the response curves in this case differ widely from those of the principal parametric resonances [11, 19, 20]. While in the latter case, the trivial branch loses its stability by super- and sub-critical pitch-fork bifurcations, in the former case, the loss of stability is due to sub- and super-critical HBs. The bifurcations in the n-t branch which have their

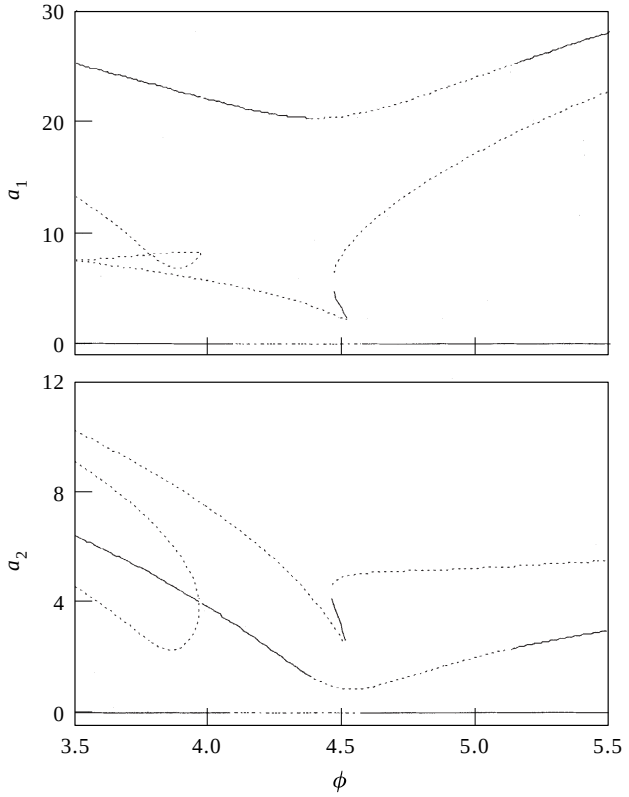

Figure 5. Frequency response curve for $\zeta_1 = \zeta_2 = \zeta_2^* \nu$; key as in Figure 3.

global origin from the trivial states differ accordingly. Similar observations can also be made from references [16, 17].

With increase in damping (Figure 3, $\nu = 2$), HBs occur in the trivial branch at $\phi = 4{\cdot}08$ and $4{\cdot}58$ and in the n-t branch at $\phi = 4{\cdot}32$ and $4{\cdot}93$. Hence, with increase in damping the trivial stability boundary is least affected, while the n-t bifurcation points shift towards the left.

The above results are obtained with different damping for the first and second modes. Considering the same damping in both the modes, as has been taken by most of the researchers, in Figure 4, with $\zeta_1 = \zeta_2 = \zeta_1^* \nu$ and for same Γ and ν as in Figure 3, these critical points in the trivial branch occur at $\phi = 4{\cdot}17$ and $4{\cdot}5$, and in the n-t branch at $\phi = 4{\cdot}4$ and $4{\cdot}9$. In Figure 4, ζ_2 has a larger value compared to that in Figure 3 which causes the shifting of the critical points and narrowing of the unstable zones in both trivial and n-t branches. Also, the n-t unstable branches of Figure 3 (except that between the HB points) coalesce to form a single unstable branch. Now, considering $\zeta_1 = \zeta_2 = \zeta_2^* \nu$ (Figure 5) for the same Γ and ν as before, in the trivial state HB occurs at $\phi = 4{\cdot}09$ and $4{\cdot}58$ and in the n-t state at $\phi = 4{\cdot}39$ and $5{\cdot}14$. As in the case of low damping (Figure 2), in this case also s-n bifurcation occurs in the n-t branch. From these four figures one may conclude that they are topologically equivalent, and hence the response

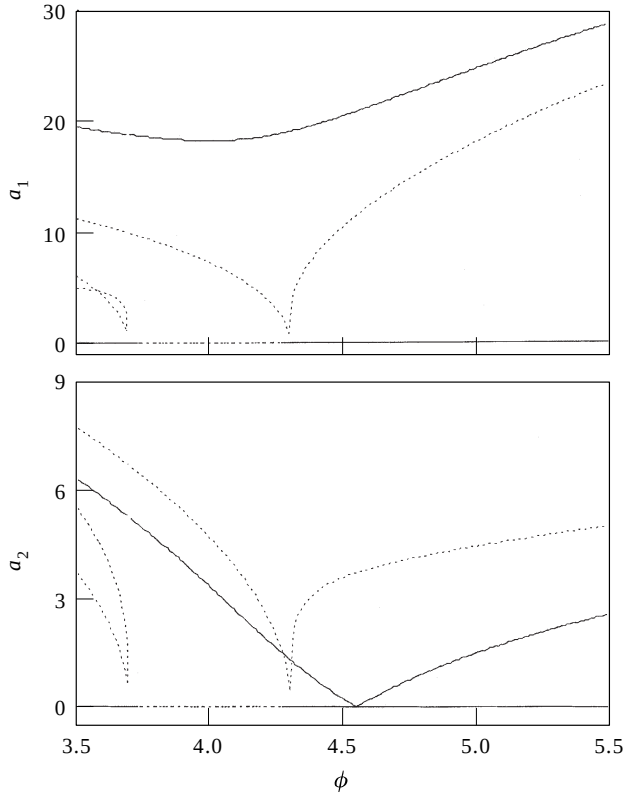

Figure 6. Frequency response curve for perfect internal detuning, $\nu = 0{\cdot}02$, with same non-linear and forcing coefficient as in Figure 2.

curves with the same damping in both modes can be obtained from the case with unequal damping by changing the values of the damping parameter ν.

Keeping other system parameters constant, with $\omega_2 = 3$ and $\zeta_1 = \zeta_2 = \zeta_2^* \nu$, Figure 6 shows the frequency response curves for $\Gamma = 10$, $\nu = 0{\cdot}02$. For the perfectly tuned internal resonance case, the n-t branch is stable and in the trivial branch HB is observed at $\phi = 3{\cdot}735$ and $4{\cdot}265$. Though the n-t stable response amplitude of the first mode increases with the frequency of external excitation, the response amplitude of the second mode decreases to zero at $\phi = 4{\cdot}55$ and again increases thereafter. At this point ($\phi = 4{\cdot}55$) a_1 has been found to have a constant value irrespective of the value of ω_2. For the negative detuning σ_2 (Figure 7), the curves are topologically equivalent to those of Figure 6. The upper n-t branch of the first mode is stable for values of negative σ_2 with a *fold* type bifurcation point at the left extreme end of the stable branch. It has been further observed that with an increase in σ_2, this critical point shifts to the left in the frequency response curve and the trivial instability zone shifts towards the right.

Figure 8 is obtained with $\mu = 4{\cdot}8$, $\beta = 0{\cdot}25$, $J = 0{\cdot}9596$ for which $\omega_2 = 3{\cdot}13526$. The critical points in the trivial branch are at $\phi = 3{\cdot}795$ and $4{\cdot}475$, and in the n-t one at $4{\cdot}16$ and $5{\cdot}02$. With an increase in μ, ω_2 decreases and when the internal

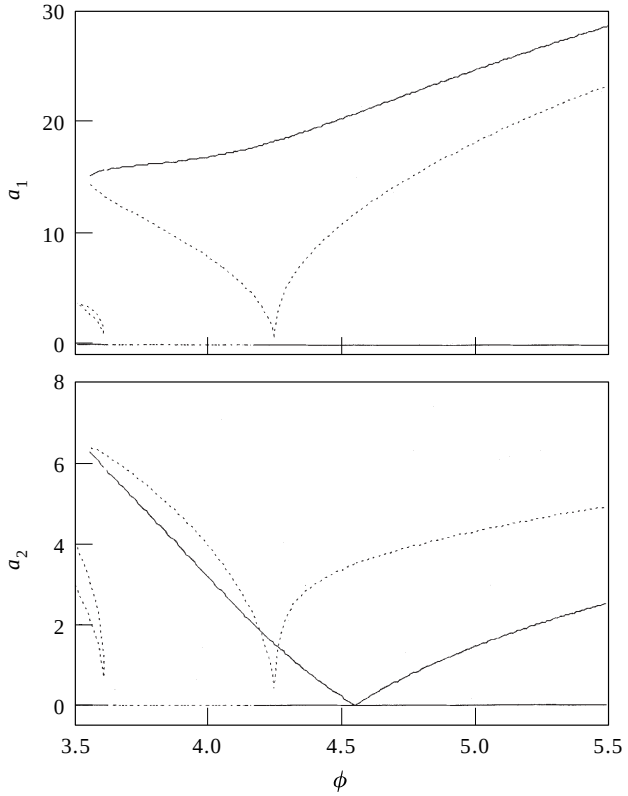

Figure 7. Frequency response curve for negative internal detuning, $\phi = 2{\cdot}9$, $\nu = 0{\cdot}02$; key as in Figure 6.

detuning σ_2 approaches zero (i.e., for near perfect internal tuning), the n-t unstable and stable branches merge to form a single branch with the Hopf bifurcation points (HBPs), as shown in Figure 9.

Table 1 shows the variation of critical points in the trivial and non-trivial branches with μ for $\beta = 0{\cdot}25$, $J = 0{\cdot}95916$, $\Gamma = 10$ and $\nu = 0{\cdot}5$. While the left Hopf bifurcation point (HBP(L)) shifts towards the left at a speed double that of the right (HBP(R)), both left and right n-t HBPs move towards the left for positive internal detuning σ_2 and towards the right for negative σ_2. For the system with very low and high values of positive σ_2, s-n bifurcation occurs but, for moderate values of positive σ_2, no bifurcation other than Hopf is found in the n-t branches. For negative σ_2, the s-n bifurcation point in the n-t branch moves towards the right with an increase in μ.

Figures 10 and 11 show the influence of β on frequency response for $\mu = 4{\cdot}0$, $\Gamma = 10$, $\nu = 0{\cdot}02$ with $\beta = 0{\cdot}23$ and $0{\cdot}27$, respectively. Also, Table 2 shows the variation of critical points with β. Unlike in the variation of μ, with increases in β, both the trivial HBPs move with almost equal speed towards the left so that the region of instability only shifts towards the left with little change in its magnitude. With changes in β, variations of the non-linear terms are found to be significant, which influence the nature and stability of the non-trivial response.

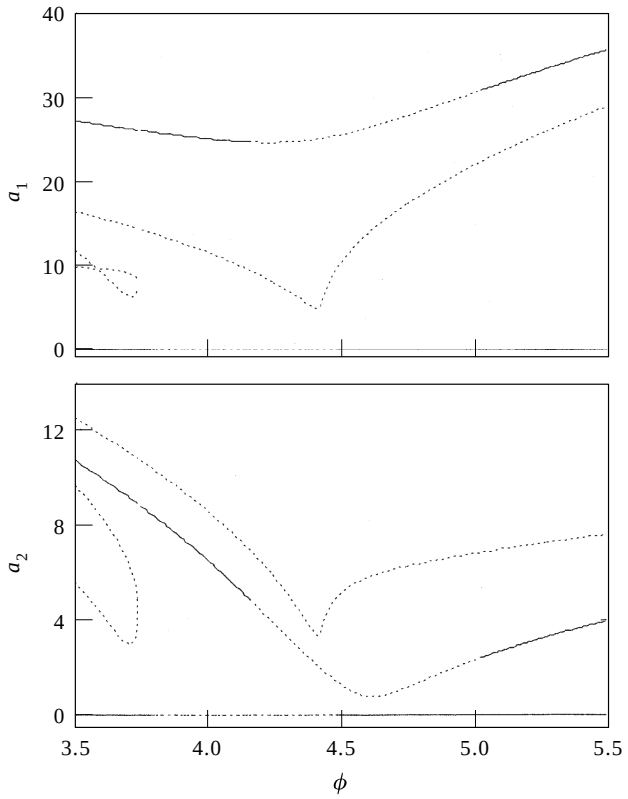

Figure 8. Frequency response curve for $\mu = 4{\cdot}8$, $\beta = 0{\cdot}25$ and $\omega_2 = 3{\cdot}13526$.

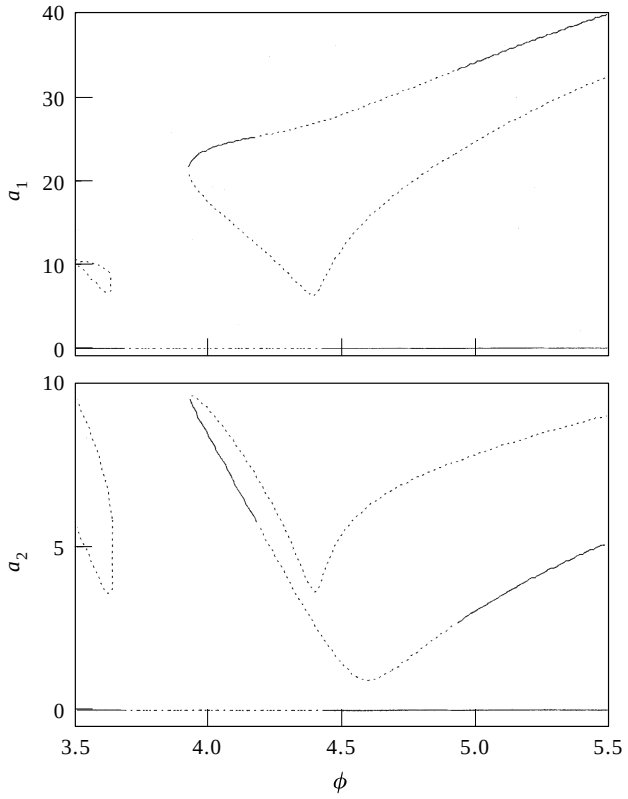

Figure 9. Frequency response curve for $\mu = 5{\cdot}4$, $\beta = 0{\cdot}25$ and $\omega = 3{\cdot}13526$.

The variation of the response amplitudes a_1 and a_2 with the amplitude of base excitation Γ is shown in Figures 12–14. For the undamped system with $\phi < \omega_1 + \omega_2$, e.g., $\phi = 4{\cdot}15$ (Figure 12(a)), there are three distinct bifurcation points, namely, the trivial HBP at $\Gamma = 7{\cdot}2$ and the two n-t s-n bifurcation points

TABLE 1

Variation of bifurcation points with μ; $\beta = 0{\cdot}25$, $\Gamma = 10$, $\nu = 0{\cdot}5$

		Trivial response		Non-trivial response		
μ	ω_2	HBP(L)	HBP(R)	HBP(L)	HBP(R)	Others
3·6	3·3506	4·08	4·62	4·37	5·18	4·53 (s-n)
4·2	3·2317	3·92	4·54	4·28	5·10	–
4·8	3·1352	3·79	4·48	4·16	5·02	–
5·4	3·057	3·69	4·43	4·18	4·93	3·93 (s-n)
6·0	2·9927	3·6	4·38	4·26	4·87	4·16 (s-n)
6·6	2·9396	3·53	4·35	4·32	4·83	4·26 (s-n)
7·2	2·8955	–	4·32	4·36	4·88	4·31 (s-n)
7·8	2·8592	–	4·3	4·39	5·09	4·34 (s-n)

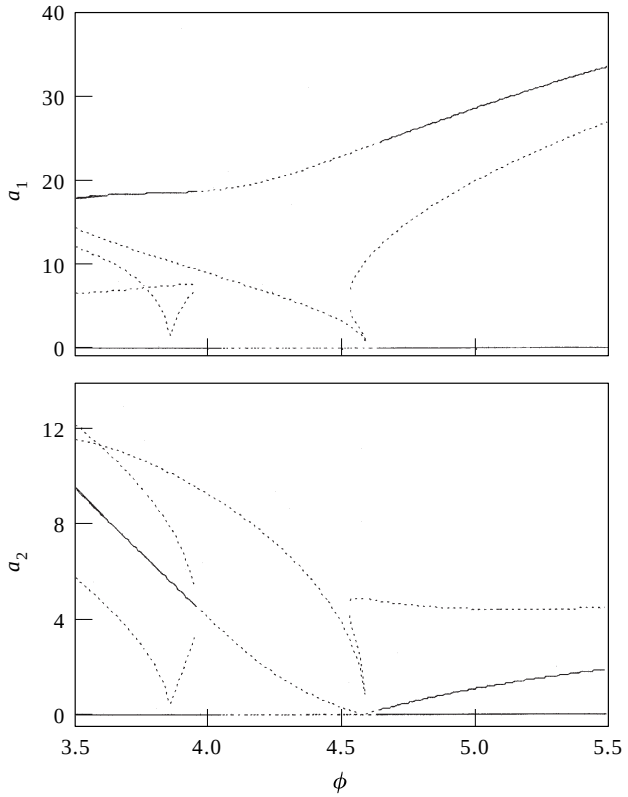

Figure 10. Frequency response curve for $\beta = 0{\cdot}23$, $\mu = 4{\cdot}0$ and $\omega_2 = 3{\cdot}33898$.

at $\Gamma = 2{\cdot}35$ and $2{\cdot}75$. With an increase in damping (Figure 12 (b)), only the trivial HBP at $\Gamma = 8{\cdot}0$ and an n-t s-n bifurcation at $\Gamma = 5{\cdot}2$ are observed. Hence, with an increase in damping, the trivial stability increases while the n-t (both stable and unstable) branches disappear for lower values of Γ and an s-n bifurcation occurs in the n-t branch.

TABLE 2

Variation of bifurcation points with β; $\mu = 4{\cdot}0$, $\Gamma = 10$, $\nu = 0{\cdot}02$

		Trivial response		Non-trivial response		
β	ω_2	HBP(L)	HBP(R)	HBP(L)	HBP(R)	Others
0·23	3·339	4·05	4·63	3·96	4·64	–
0·24	3·298	4·0	4·59	4·0	–	–
0·25	3·268	3·97	4·57	4·32	5·14	–
0·26	3·249	3·96	4·54	4·57		4·49 (s-n)
0·27	3·242	3·95	4·53	4·76		4·5 (s-n)
0·28	3·244	3·96	4·52	4·89		

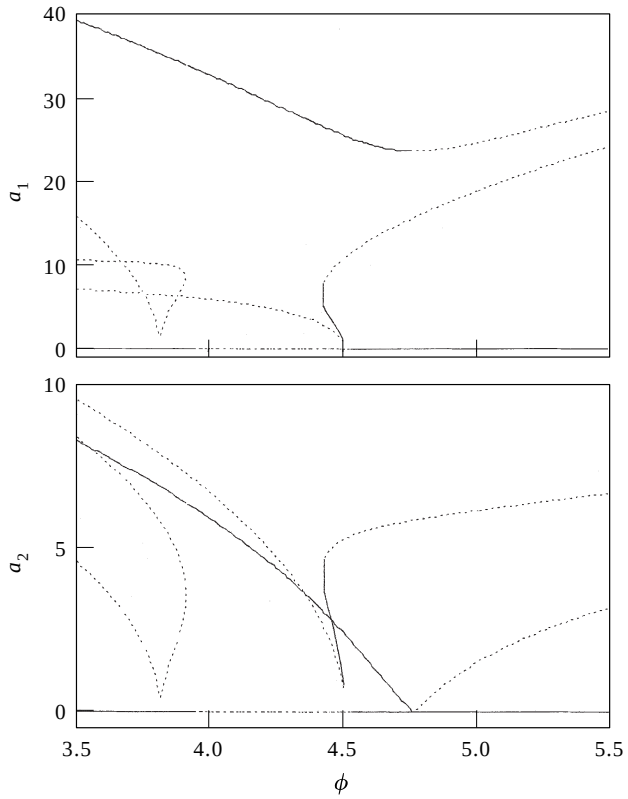

Figure 11. Frequency response curve for $\beta = 0{\cdot}27$, $\mu = 4{\cdot}0$ and $\omega_2 = 3{\cdot}2415$.

With $\phi = \omega_1 + \omega_2$ (Figure 13), for the undamped case, the trivial response is unstable and in the n-t branch stability is restored by HB at $\Gamma = 5{\cdot}2$. Also, as in the previous case, another n-t branch becomes unstable by s-n bifurcation at $\Gamma = 5{\cdot}7$. Thus, with an increase in Γ, the response jumps up at this turning point for the first mode and jumps down for the second mode, while for reduction in Γ, the response jumps down for the first mode and jumps up for the second mode at the HBP from one stable n-t branch to another. Hence, this region between the Hopf and s-n bifurcation points is the region exhibiting *bistability* and *hysteresis phenomenon* as the response depends on the direction of sweep of the control parameter Γ. For $\nu = 2$, the trivial branch remains stable until $\Gamma = 4{\cdot}7$ where it loses its stability by HB. An interesting *ring* is formed with the upper stable and lower unstable halves joined by s-n bifurcation points at $\Gamma = 6{\cdot}5$ and $8{\cdot}3$. So the system remains unstable from $\Gamma = 4{\cdot}7$ to $6{\cdot}5$ and $8{\cdot}3$ to $11{\cdot}2$, where the stability is restored by HB. Thus, it is evident that damping has a *destabilizing effect* on the system response. One may observe that, for $6{\cdot}5 \leqslant \Gamma \leqslant 8{\cdot}3$, $a_2 > a_1$; but, after the HBP, $a_2 \ll a_1$. Although the energy flows from the higher mode to the lower one in the cubic non-linear system, there is a tendency of the higher mode to *saturate*.

Now with $\phi > \omega_1 + \omega_2$, e.g., $\phi = 4{\cdot}5$ for an undamped system (Figure 14(a)), the trivial branch becomes unstable by HB at $\Gamma = 6{\cdot}7$, while at $\Gamma = 5{\cdot}9$ both stable and unstable n-t branches pitch-forked from the trivial branch. The n-t

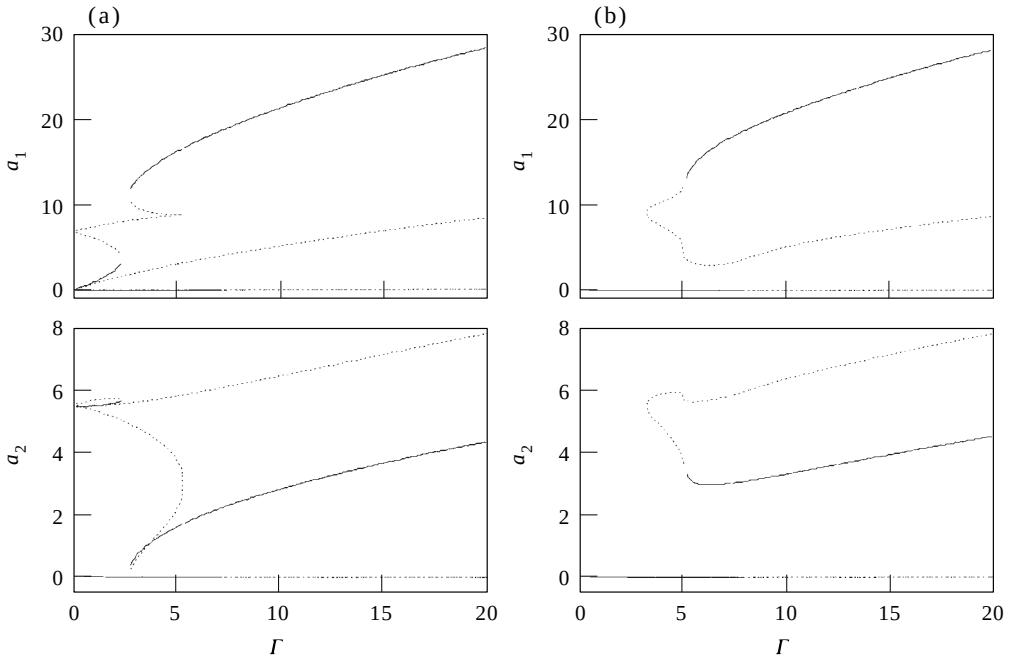

Figure 12. Variation of steady state response with Γ for $\phi = 4{\cdot}15$. (a) $\nu = 0$, (b) $\nu = 2$.

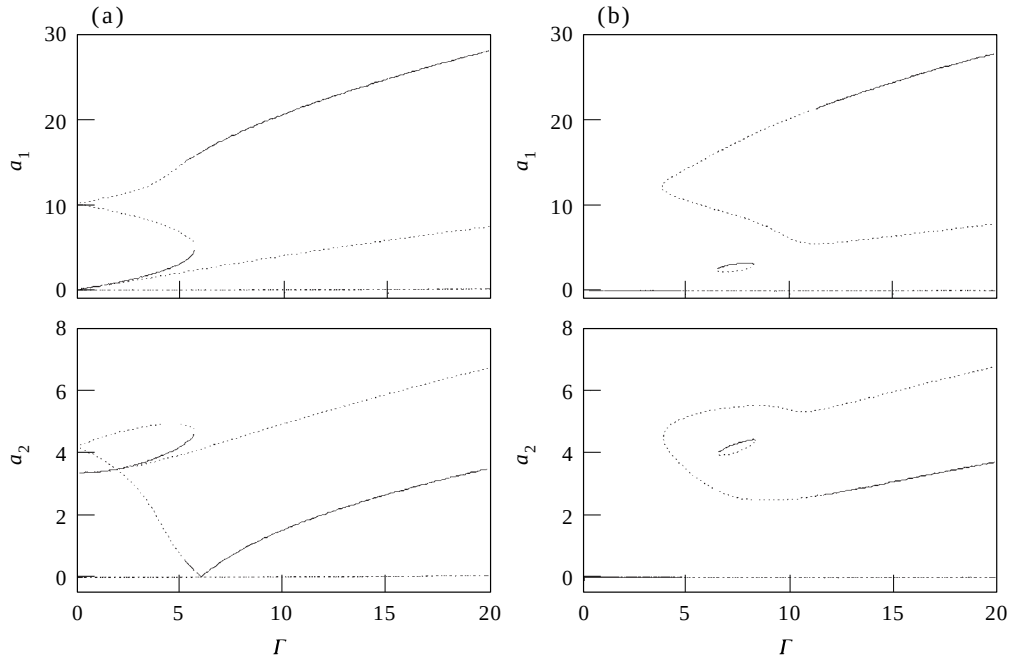

Figure 13. Force response curve for $\phi = 4{\cdot}33179$. (a) $\nu = 0$; (b) $\nu = 2$.

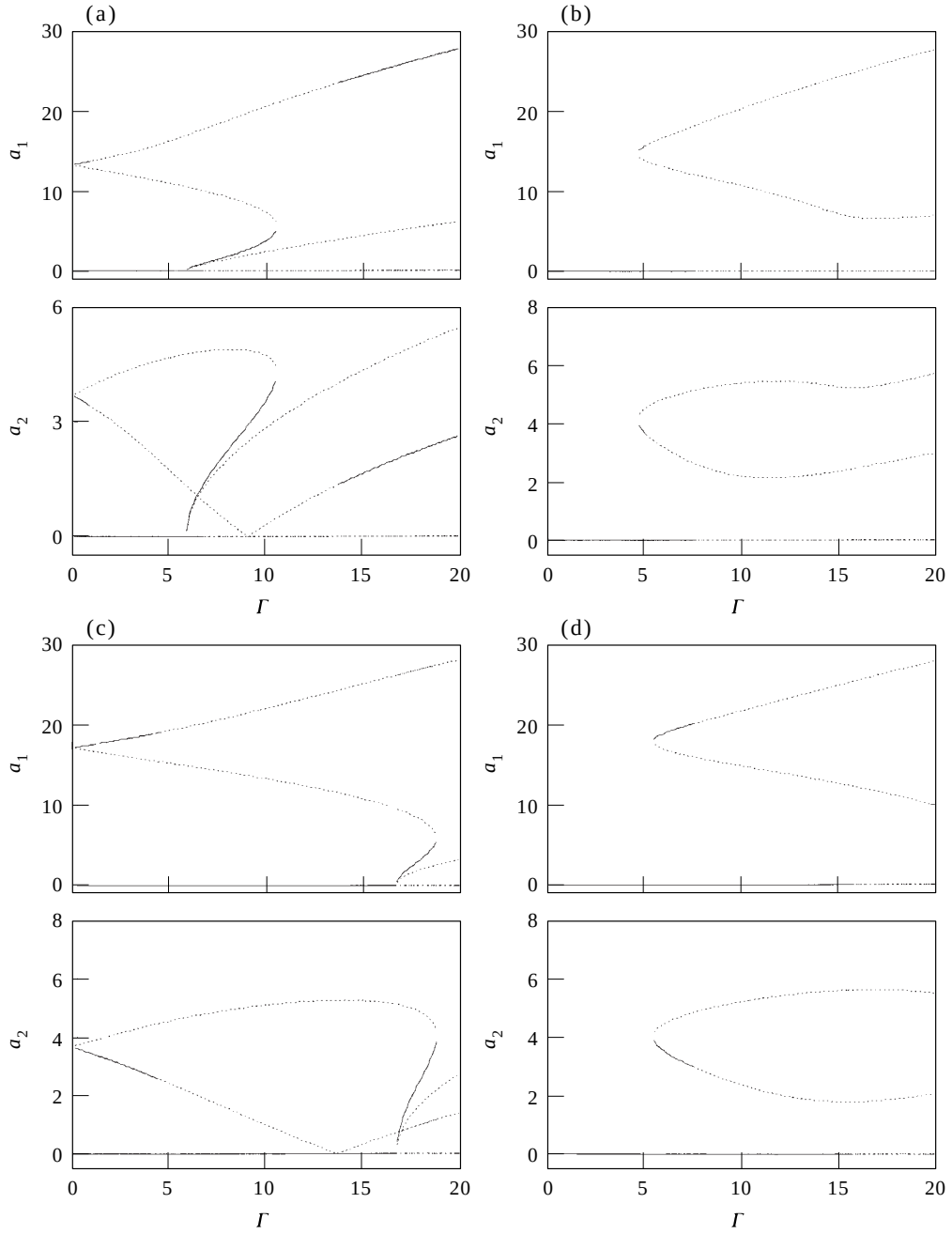

Figure 14. Variation of steady state response with Γ. (a) $\phi = 4{\cdot}5$, $\nu = 0$; (b) $\phi = 4{\cdot}5$, $\nu = 2$; (c) $\phi = 4{\cdot}75$, $\nu = 0$; (d) $\phi = 4{\cdot}75$, $\nu = 2$.

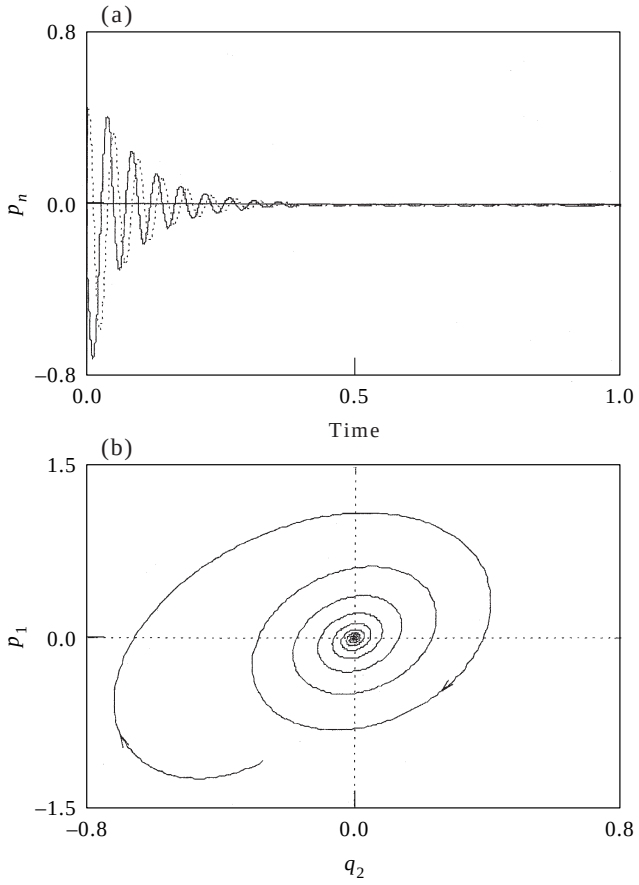

Figure 15. (a) Time history showing trivial fixed point response, obtained by directly integrating equations (37)–(39) at $\phi = 4$; ——, p_1; . . . . . , p_2. (b) Projection of the trajectory in p_1–q_2 plane. Key as in Figure 3.

branches become unstable at $\Gamma = 10{\cdot}5$ by s-n and at $\Gamma = 0{\cdot}9$ and $13{\cdot}7$ by HB. In this case also no stable branch exists between $\Gamma = 10{\cdot}5$ and $13{\cdot}7$. With an increase in damping ($\nu = 2$, Figure 14(b)), the trivial branch becomes unstable at $\Gamma = 7{\cdot}6$ and the n-t branch is stable between $\Gamma = 4{\cdot}7$ and $5{\cdot}1$. So the system-stability depends almost exclusively on the stability of the trivial state which increases with an increase in damping, but the stability of the overall system decreases. With a further increase in ϕ, e.g., $\phi = 4{\cdot}75$ for an undamped system (Figure 14(c)), the trivial response remains stable until the trivial HBP at $16{\cdot}7$ and in the n-t branches s-n bifurcations at $\Gamma = 0{\cdot}1$ and $18{\cdot}7$ and HB at $\Gamma = 4{\cdot}6$ are observed. Since no stable branch exists to the right of the turning point at $\Gamma = 18{\cdot}7$, for increasing values of Γ the system suddenly becomes unstable indicating the *blue sky catastrophe phenomena*. For a damped case ($\nu = 2$, Figure 14(d)), the trivial branch becomes unstable at $\Gamma = 15{\cdot}7$ and the n-t branch remains stable between $\Gamma = 5{\cdot}5$ and $7{\cdot}6$. Hence, for $\phi \gg \omega_1 + \omega_2$, with an increase in damping, both trivial and n-t stability decrease.

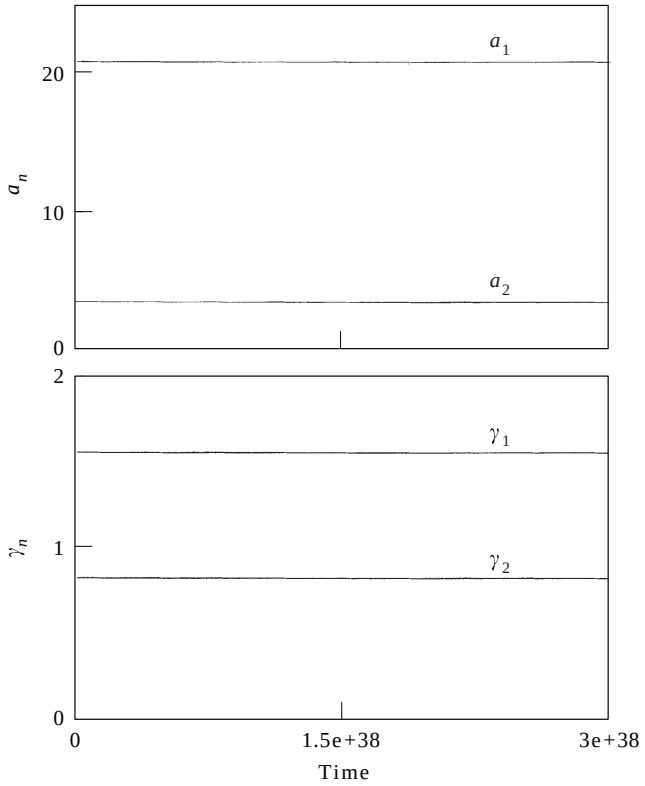

Figure 16. The results of time integration showing non-trivial fixed point response for $\Gamma = 10$; key as in Figure 12(b).

The response curves can also be obtained by directly integrating the reduced equations (25)–(28) or (37)–(39). Figure 15(a) shows the time response plot for the trivial fixed point at $\phi = 4$, $\Gamma = 10$, $\nu = 2$ (Figure 3). As the trajectory in p_1, q_2 plane (Figure 15(b)), moves towards the fixed point with time $\tau \to \infty$, the fixed point is found to be stable. The time response for $\phi = 4{\cdot}15$, $\Gamma = 10$, $\nu = 2$ is shown in Figure 16 indicating a stable n-t fixed point ($a_1 = 20{\cdot}787$, $a_2 = 3{\cdot}3373$, $\gamma = 1{\cdot}555$, $\gamma_2 = 0{\cdot}826$) which is in good agreement with that in Figure 12(b). In Figure 17(a), the periodic responses at $\phi = 4{\cdot}33179$, $\Gamma = 10$, $\nu = 0$ arising due to the super-critical HB (Figure 2) are shown. Figure 17(b) shows the projection of the corresponding limit cycle trajectory on the a_1–a_2 plane. The non-linear responses in the unstable regions which may be periodic, quasi-periodic or chaotic are studied in Part II of this paper.

4. CONCLUSIONS

The non-linear response of a vertically base-excited slender beam with a lumped mass is studied using the method of multiple scales. The stability and bifurcation of the trivial and non-trivial branches for different values of damping ν, amplitude Γ and frequency ϕ of base excitation are studied for various values of mass ratio μ and location parameter β. HB is found to occur in the trivial

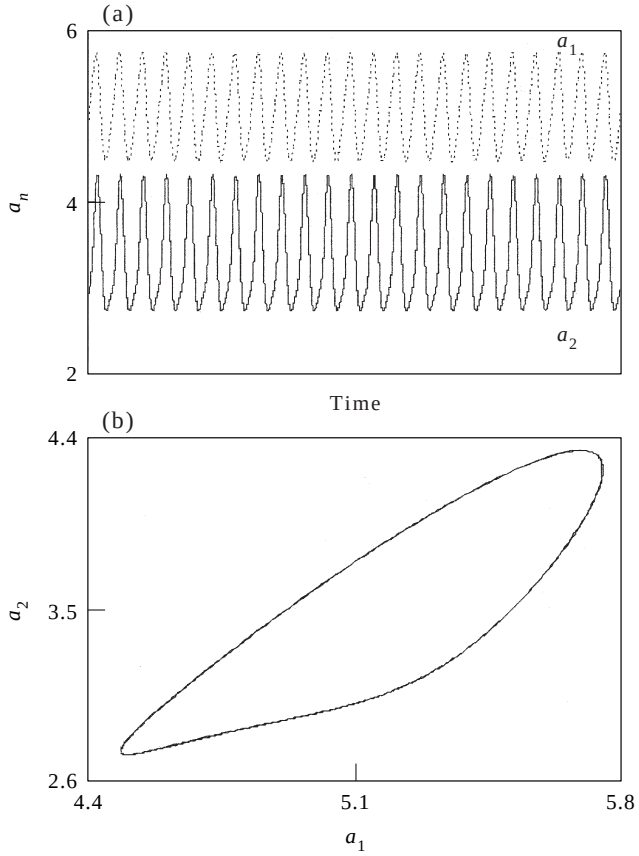

Figure 17. The results of time integration showing periodic response for $\phi = \omega_1 + \omega_2$. (a) Time response plot, (b) projection of limit cycle on the a_1–a_2 plane. Key as in Figure 2.

branch and no symmetry-breaking pitch-fork bifurcation is observed in the combination resonance. Also, non-trivial branch contains Hopf bifurcation points and sometimes saddle-node bifurcation points which vary with Γ and ν. Though topologically equivalent response curves are obtained for different values of μ and β, the stability of the response curve differs very much with the variation of β which alters the non-linear coefficients considerably. With an increase in damping the stability of the trivial state increases, but the overall stability of the system decreases for $\phi > \omega_1 + \omega_2$ and, for $\phi < \omega_1 + \omega_2$, some of the stable and unstable branches disappear; but the system remains stable with the trivial and/or non-trivial stable branches. For lower values of damping, the system contains a number of solutions and multiple jump-phenomena are observed. Hysteresis, saturation and blue sky catastrophe phenomena, fractional harmonic pair and energy transfer from the higher mode to the lower mode are observed in this system.

REFERENCES

1. V. V. Bolotin 1964 *The Dynamic Stability of Elastic Systems*. San Francisco: Holden-Day.

2. A. H. NAYFEH and D. T. MOOK 1979 *Nonlinear Oscillations*. New York: Wiley-Interscience.
3. W. SZEMPLIN'SKA-STUPNICA 1990 *The Behaviour of Non-linear Vibrating Systems, Vol* 1 *Fundamental Concepts and Methods*, *Application to Single Degree of Freedom Systems*, *Vol* 2 *Advance Concepts and Applications to Multi Degrees of Freedom Systems*. London: Kluwer Academic.
4. M. P. CARTMELL 1990 *Introduction to Linear*, *Parametric and Non-linear Vibrations*. London: Chapman & Hall.
5. A. H. NAYFEH and B. BALACHANDRAN 1989 *American Society of Mechanical Engineers, Applied Mechanics Review* **42**, S175–S201. Modal interactions in dynamical and structural systems.
6. K. G. VALEEV 1963 *Journal of Applied Mathematics and Mechanics* **6**, 1745–1769. On the danger of combination resonance.
7. J. DUGUNDJI and V. MUKHOPADHYAY 1973 *Journal of Applied Mechanics* **40**, 693–698. Lateral bending-torsion vibrations of a thin beam under parametric excitation.
8. W. K. TSO and K. G. ASMIS 1974 *International Journal of Non-Linear Mechanics* **9**, 269–277. Multiple parametric resonance in a non-linear two-degree-of-freedom system.
9. N. SRI NAMCHCHIVAYA and W. M. TIEN 1989 *International Journal of Non-linear Mechanics* **24**, 197–208. Non-linear dynamics of supported pipe conveying pulsating fluid II. Combination resonance.
10. K. G. ASMIS and W. K. TSO 1972 *American Society of Mechanical Engineers*, *Journal of Applied Mechanics* **39**, 832–834. Combination and internal resonance in a non-linear two-degree-of freedom system.
11. E. G. TEZAK, D. T. MOOK and A. H. NAYFEH 1978 *American Society of Mechanical Engineers*, *Journal of Machine Design* **100**, 651–655. Nonlinear analysis of the lateral response of columns to periodic loads.
12. A. H. NAYFEH 1983 *Journal of Sound and Vibration* **88** 547–557. The response of two-of-freedom systems with quadratic non-linearities to a parametric excitation.
13. A. H. NAYFEH and A. E. S. JEBRILL 1987 *Journal of Sound and Vibration* **115**, 83–101. The response of two-degree-of freedom systems with quadratic and cubic nonlinearities to multifrequency excitations.
14. A. H. NAYFEH 1983 *Journal of Sound and Vibration* **90**, 237–244. The response of multidegree-of-freedom systems with quadratic non-linearities to a harmonic parametric resonance.
15. M. P. CARTMELL and J. W. ROBERTS 1988 *Journal of Sound and Vibration* **123**, 81–101. Simultaneous combination resonances in an autoparametrically resonant system.
16. A. H. NAYFEH and L. D. ZAVODNEY 1986 *Journal of Sound and Vibration* **107**, 329–350. The response of two degree-of-freedom systems with quadratic non-linearities to a combination parametric resonance.
17. D. A. STREIT, A. K. BAJAJ and C. M. KROUSGRILL 1988 *Journal of Sound and Vibration* **124**, 297–314. Combination parametric resonance leading to periodic and chaotic response in two-degree-of-freedom systems with quadratic non-linearities.
18. A. H. NAYFEH and P. F. PAI 1989 *International Journal of Non-linear Mechanics* **24**, 139–158. Non-linear non-planar parametric responses of an in-extensional beam.
19. R. C. KAR and S. K. DWIVEDY 1998 *International Journal of Non-linear Mechanics* **34**, 515–529. Nonlinear dynamics of a slender beam carrying a lumped mass to principal parametric and internal resonances.
20. L. D. ZAVODNEY and A. H. NAYFEH 1989 *International Journal of Non-linear Mechanics* **24**, 105–125. The non-linear response of a slender beam carrying a lumped mass to principal parametric excitation: theory and experiment.

21. W. H. PRESS, S. A. TEUKOLSKY, W. T. VETTERLING and B. P. FLANNERY 1993 *Numerical Recipes in Fortran*. Cambridge: Cambridge University Press; first Indian edition.

APPENDIX

$$h_{11} = \int_0^1 \psi_n^2 \, \mathrm{d}x, \; h_{12} = \int_0^1 \delta(x-\beta)\psi_n^2 \, \mathrm{d}x,$$

$$h_{13} = \int_0^1 \delta(x-\beta)(\psi_{nx})^2 \, \mathrm{d}x = \psi_{nx}^2(\beta), \; h_{21} = \int_0^1 \psi_n^2 \, \mathrm{d}x = h_{11},$$

$$R_n = h_{11} + \mu h_{12} + J\lambda^2 h_{13}, \; \zeta_n = \zeta_n^* \nu = \varepsilon\left(\frac{ch_{21}}{2\varepsilon R_n \rho \theta_1}\right)\nu,$$

$$h_{31} = \int_0^1 \psi_n^2 \, \mathrm{d}x, \; h_{32} = \int_0^1 \delta(x-\beta)\psi_n^2 \, \mathrm{d}x = h_{12}\,,$$

$$h_{33} = \int_0^1 (1-x)\psi_{nx}^2 \, \mathrm{d}x, \; h_{34} = \int_0^1 \int_x^1 \delta(\xi-\beta) \, \mathrm{d}\xi \psi_{nx}^2 \, \mathrm{d}x,$$

$$\theta_n^2 = \frac{EI\kappa_n^4}{\rho L^4 R_n}(h_{31} + \mu h_{32}) - \frac{g}{LR_n}(h_{33} + \mu h_{34}),$$

$$f_{nm} = f_{nm}^* \Gamma/\varepsilon = \frac{\Omega^2 Z_o}{\varepsilon \theta_1^2 R_n L}(h_{33} + \mu h_{34}),$$

$$h_{41} = \frac{1}{2}\int_0^1 \psi_k \psi_{lx} \psi_{mx} \psi_n \, \mathrm{d}x, \; h_{42} = \frac{1}{2}\int_0^1 \delta(x-\beta)\psi_k \psi_{lx} \psi_{mx} \psi_n \, \mathrm{d}x,$$

$$h_{43} = 3\int_0^1 \psi_{kx} \psi_{lxx} \psi_{mxxx} \psi_n \, \mathrm{d}x + \int_0^1 \psi_{kxx} \psi_{lxx} \psi_{mxx} \psi_n \, \mathrm{d}x,$$

$$\alpha_{klm}^n = \frac{EI\lambda^2}{\varepsilon \rho L^4 R_n \theta_1^2}\{\kappa_k^4(h_{41} + \mu h_{42}) + h_{43}\},$$

$$h_{51} = \int_0^1 \left\{ \int_x^1 \left(\int_0^\xi \psi_{l\eta} \psi_{m\eta} \, \mathrm{d}\eta \right) \mathrm{d}\xi \right\} \psi_{kx} \psi_{nx} \, \mathrm{d}x,$$

$$h_{52} = \left(\int_0^\beta \psi_{lx}\psi_{mx}\,\mathrm{d}x\right)\left(\int_0^\beta \psi_{kx}\psi_{nx}\,\mathrm{d}x\right),$$

$$h_{53} = \{\psi_{kx}\psi_{lx}\psi_{mx}\psi_{nx}\}_{x=\beta},$$

$$\beta^n_{klm} = \frac{\lambda^2}{\varepsilon R_n}\{h_{51} + \mu h_{52} + J\lambda^2 h_{53}\},$$

$$h_{61} = h_{51},$$

$$h_{62} = \frac{1}{2}\int_0^1 \psi_{kx}\psi_{lx}\psi_m\psi_n\,\mathrm{d}x - \int_0^1 \psi_{kx}\psi_{lxx}\left(\int_x^1 \psi_m\,\mathrm{d}\xi\right)\psi_n\,\mathrm{d}x,$$

$$h_{63} = h_{52},$$

$$h_{64} = \frac{1}{2}[\psi_{kx}\psi_{lx}\psi_m\psi_n]_{x=\beta} - \psi_m(\beta)\int_0^\beta \psi_{kx}\psi_{lxx}\psi_n\,\mathrm{d}x,$$

$$h_{65} = \frac{1}{2}h_{53},$$

$$\gamma^n_{klm} = \frac{\lambda^2}{\varepsilon R_n}[h_{61} - h_{62} + \mu(h_{63} - h_{64}) + J\lambda^2 h_{65}].$$

Expression for α_{enj}, Q_{131}, Q_{31}

$$\alpha_{enj} = \alpha_{nj} + \beta_{nj} + \gamma_{nj},$$

$$\alpha_{nj} = 3\alpha^n_{nnn}, \quad \text{for } j = n$$

$$= 2(\alpha^n_{njj} + \alpha^n_{jjn} + \alpha^n_{jnj}), \quad \text{for } j \neq n,$$

$$\beta_{nj} = \omega_n^2\beta^n_{nnn}, \quad \text{for } j = n$$

$$= 2\omega_j^2\beta^n_{njj}, \quad \text{for } j \neq n,$$

$$\gamma_{nj} = -3\omega_n^2\gamma^n_{nnn}, \quad \text{for } j = n$$

$$= -2\{\omega_j^2(\gamma_{jnj}^n + \gamma_{njj}^n) + \omega_n^2\gamma_{jjn}^n\}, \quad \text{for } j \neq n,$$

$$Q_{131} = \alpha_{121}^1 + \alpha_{211}^1 + \alpha_{112}^1 - \omega_1^2\beta_{211}^1 + \omega_1\omega_2(\beta_{121}^1 + \beta_{112}^1) - \{\omega_1^2(\gamma_{211}^1 + \gamma_{121}^1) + \omega_2^2\gamma_{112}^1\},$$

$$Q_{31} = \alpha_{111}^2 - \omega_1^2(\beta_{111}^2 + \gamma_{111}^2).$$

The linear undamped mode shape $\psi_n(x)$ can be written in non-dimensional form as

$$\psi_n(x) = [(\sin\kappa_n x - \sinh\kappa_n x) - \Lambda(\cos\kappa_n x - \cosh\kappa_n x)] + U(x-\beta)\{(h_1 - \Lambda h_2)[\sin\kappa_n(x-\beta) - \sinh\kappa_n(x-\beta)] + (h_3 - \Lambda h_4)[\cos\kappa_n(x-\beta) - \cosh\kappa_n(x-\beta)]\},$$

where h_1, h_2, h_3, h_4 and Λ are defined in reference [20], U is the unit step function, $\psi_n(x)$ is the eigenfunction of the *nth* mode, and Θ_n is the *nth* linear natural frequency of the system which is given by

$$\Theta_n^2 = \frac{EI}{\rho}\left(\frac{\kappa_n}{L}\right)^4.$$

κ_n is the eigenvalue of the nth mode of vibration obtained from the solution of the transcendal equation

$$\frac{4(h_1h_4 - h_2h_3)}{\lambda^2\mu J} + 2\kappa^4[1 - \cos\ \kappa\beta\cosh\ \kappa\beta] + \frac{2\kappa^3}{\mu}[h_1(\sin\kappa\beta + \sinh\kappa\beta) + h_2(\cos\kappa\beta - \cosh\kappa\beta)] + \frac{2\kappa}{J\lambda^2}[h_4(\sin\kappa\beta - \sinh\kappa\beta) - h_3(\cos\kappa\beta - \cosh\kappa\beta)] = 0.$$